colony-stimulating factor (GM-CSF)– and interleukin-4 (IL-4)–treated CD1+ monocytes and *M. leprae* sonicate. After establishment of LDN5, cultures were maintained in IL-2–supplemented medium and periodically stimulated with allogenic CD1+ APCs and *M. phlei* sonicate. Flow cytometric analysis of LDN5 revealed positivity for αβ TCR, but not CD4 or CD8β. T cell culture methods, proliferation assays, and cytolysis assays have been described (*6*).

8. *Mycobacterium phlei*, *M. tuberculosis H37Ra*, *M. fortuitum*, *M. smegmatis*, and *M. bovis BCG* were cultivated in 7H9 medium (Difco) supplemented with 0.05% Tween-80 and 1% glucose, mannose, or galactose. Organic extracts (1×) were made by shaking 7.5 mg of lyophilized bacteria per 1 ml of chloroform:methanol (2:1) at 20°C for 2 hours. Sonicates (1×) were made by probe sonication of 10 mg of bacteria per milliliter of phosphate-buffered saline, subsequently clarified by centrifugation as described (*6*). Mycolyl glycolipids were purified with preparative silica TLC in solvent A (60:16:2 chloroform:methanol:water) and extraction from silica into chloroform:methanol (2:1) or by eluting an open 2 cm by 20 cm silica column serially with chloroform and acetone in a stepwise gradient. The antigenic glycolipid eluted in 30% acetone in chloroform.
9. P. J. Brennan, D. P. Lehane, D. W. Thomas, *Eur. J. Biochem.* **13**, 117 (1969). The purified antigenic glycolipid was hydrolyzed, and the resulting products were partitioned between aqueous and organic phases. Organic soluble products were derivatized with phenacyl bromide and coeluted on C18 reversed-phase HPLC with *M. tuberculosis* mycolic acids as described (*4*). We determined the carbohydrate structure by methylating the reducing end of the intact glycolipid (0.5 N HCL in methanol at 65°C for 2 hours), followed by alkaline hydrolysis. Aqueous-phase products were acetylated and compared with acetylated methyl glycosides of authentic glucose and other carbohydrates by GC.
10. G. S. Besra and D. Chatterjee, in *Tuberculosis, Pathogenesis, Protection and Control*, B. R. Bloom, Ed. (American Society for Microbiology, Washington, DC, 1994), pp. 285–306. ESI-MS was performed on a Quattro II triple quadrupole mass spectrometer in the positive mode with samples in chloroform:methanol (2:1) at a flow rate of 2 to 4 μl/min.
11. We hydrolyzed *M. phlei*, *M. tuberculosis* (Sigma), and synthetic (Ribi) α,α′-trehalose dimycolate to yield GMM by drying on glass and treating with 2 M trifluoroacetic acid (TFA) at 121°C for 2 hours [G. S. Besra, T. Sievert, R. L. Lee, A. Slayden, P. J. Brennan, *Proc. Natl. Acad. Sci. U.S.A.* **91**, 12737 (1994)]. The yield of the resulting glycolipids was determined by comparison of TLC with authentic GMM standards. ESI-MS analysis revealed ions of the expected *m/z* for GMM.
12. *Mycobacterium bovis BCG* and *M. tuberculosis* mycolic acids contain cyclopropyl groups, whereas *M. smegmatis* mycolic acids contain double bonds in place of cyclopropyl groups [K. Kaneda *et al.*, *J. Gen. Microbiol.* **134**, 2213 (1988); Y. Yuan, R. E. Lee, G. S. Besra, J. T. Belisle, C. E. Barry, *Proc. Nat. Acad. Sci. U.S.A.* **92**, 6630 (1995)]. These species produce mycolic acids containing either no R group (α and α′ mycolates) or named R groups as follows: *M. tuberculosis* (α, keto, methoxy); BCG (α, keto); *M. phlei* (α, wax-ester, and possibly small amounts of keto); and *M. fortuitum* and *M. smegmatis* (α, α′, epoxy) [(*18*); R. E. Lee, P. J. Brennan, G. S. Besra, *Curr. Top. Microbiol. Immunol.* **215**, 1 (1996)].
13. Previously described methods for trehalose monomycolate purification, mycolic acid synthesis, TBDMS derivatization, and hexose-6-*O*-acyl preparation [A. K. Datta, K. Takayama, M. A. Nashed, L. Anderson, *Carbohydr. Res.* **218**, 95 (1991)] were used, except that the appropriate lipid [3-hydroxypalmitate (Matreya), tetradecylhexadecanoate (Wako), or triacontanoate (Sigma)] or carbohydrate [glucose, mannose, or galactose (Sigma)] were substituted in the reactions. "Natural" hexose mycolates were isolated from *M. phlei* grown in glucose-, galactose-, or mannose-supplemented media [Y. Natsuhara, S. Oka, K. Kaneda, Y. Kato I. Yano, *Cancer Immunol. Immunother.* **31**, 99 (1990)]. Glycerol monomycolate (*18*), and arabinomycolate were purified from *M. tuberculosis* [G. S. Besra *et al.*, *Proc. Natl. Acad. Sci. U.S.A.* **91**, 12735 (1994)]. Lipid structures were confirmed by ESI-MS and TLC. Nuclear magnetic resonance analysis of semisynthetic hexose monomycolates (Bruker ACE-300) revealed a low-field chemical shift of H-6_a (δ 4.51, doublet) and H-6_b (δ 4.06, double doublet) indicative of acylation at the position 6 hydroxyl.
14. LDN5 failed to respond to glucopsychosine, *n*-lignoceroyldihydroglucocerebroside, *n*-palmitoyldihydroglucocerebroside, *n*-stearoyldihydroglucocerebroside (Sigma), and glucose-6-*O*-triacontanoate (*13*) at all doses tested.
15. LDN5 recognition of GMM appeared to require antigen uptake and processing, as was the case for CD1b-restricted recognition of mycolic acid (*3*, *4*) and lipoglycans (*5*). Treatment of macrophages with 25 mM chloroquine reduced the proliferative response of LDN5 to GMM by 52% compared with macrophages pulsed with antigen before chloroquine treatment. Treatment of macrophages with 0.025% glutaraldehyde before antigen exposure abolished the response of LDN5 to GMM (*3*).
16. Z.-H. Zeng *et al.*, *Science* **277**, 339 (1997).
17. The CD1-lipid antigen association is predicted to occur with an orientation similar to that of phosphatidylcholine in the hydrophobic cavity (576 A^2 surface area) of bactericidal permeability-increasing protein (BPI) in which the acyl chains are buried deeply and the charged phosphate group is exposed to aqueous solvent [L. J. Beamer, S. F. Carroll, D. Eisenberg, *Science* **276**, 1861 (1997)]. The CD1 groove is larger (1310 A^2 surface area) and more extended than that of BPI, suggesting that the acyl chains of CD1 ligands may lie in an extended conformation rather that parallel as is the case for BPI (*16*). These interactions contrast with that of free fatty acids with fatty acid binding protein in which the free fatty acid is oriented with the charged carboxylate at the bottom of the groove stabilized by basic amino acid side chains [J. Eads, J. C. Sacchettini, A. Kromminga, J. I. Gordon, *J. Biol. Chem.* **268**, 26375 (1993)].
18. D. E. Minnikin, S. M. Minnikin, J. H. Parlett, M. Goodfellow, M. Magnusson, *Arch. Microbiol.* **139**, 225 (1984).
19. We thank C. Morita, M. Brenner, C. Barry, B. Segelke, and I. Wilson for helpful discussions and for sharing unpublished data. Supported by NIH–National Institute of Arthritis and Musculoskeletal and Skin Diseases grant AR01988 (D.B.M.), NIH grants GM54045 and RR10888 (B.B.R., S.Y., and V.N.R.), and National Institute of Allergy and Infectious Diseases (NIAID)–NIH grants AI18357 and AI35220 (M.R.G. and G.S.B.). S.A.P. is an Arthritis Foundation Investigator and is supported by NIH-NIAID grant AI40135 and a grant from the American Cancer Society.

25 June 1997; accepted 29 August 1997

Structure-Based Analysis of Catalysis and Substrate Definition in the HIT Protein Family

Christopher D. Lima, Michael G. Klein, Wayne A. Hendrickson

The histidine triad (HIT) protein family is among the most ubiquitous and highly conserved in nature, but a biological activity has not yet been identified for any member of the HIT family. Fragile histidine triad protein (FHIT) and protein kinase C interacting protein (PKCI) were used in a structure-based approach to elucidate characteristics of in vivo ligands and reactions. Crystallographic structures of apo, substrate analog, pentacovalent transition-state analog, and product states of both enzymes reveal a catalytic mechanism and define substrate characteristics required for catalysis, thus unifying the HIT family as nucleotidyl hydrolases, transferases, or both. The approach described here may be useful in identifying structure-function relations between protein families identified through genomics.

Human FHIT and PKCI proteins are members of the ubiquitous protein family HIT, which denotes a conserved histidine triad (His-x-His-x-His) sequence motif (*1*). HIT protein sequences have been identified independently and through genomics in Prokaryae, Archae, and Eukaryae [(*1*, *2*) and references therein]. Members can be aligned to reveal at least two subfamilies. One subfamily, of which human PKCI is a member, is found throughout evolution and is characterized by a highly conserved COOH-terminal sequence and greater than 94% amino acid sequence identity overall between known mammalian homologs. We previously described the identification, cloning, and structure determination of human PKCI in its unliganded form (*3*). Human FHIT, whose gene resides in a fragile locus on human chromosome 3 (*4*), is a member of a divergent eukaryotic HIT subfamily that differs significantly from the more conserved subfamily (~20% identity) by deviations at NH_2- and COOH-termini. Disruption of the *FHIT* gene is associated with human cancers (*4*), but definitive evidence supporting its role as a tumor suppressor has yet to be elucidated. We recently reported the three-dimensional structure of FHIT and its complex with a nucleoside ligand (*2*). A core domain of ~100 amino acids is similar among all HIT family members; PKCI and FHIT share 20.7% identity over a 110–amino acid overlap.

Characterized HIT proteins exist as ho-

C. D. Lima, Department of Biochemistry and Molecular Biophysics, Columbia University, New York, NY 10032, USA.
M. G. Klein, Herbert Irving Cancer Center and Institute of Human Nutrition, New York, NY 10032, USA.
W. A. Hendrickson, Department of Biochemistry and Molecular Biophysics and Howard Hughes Medical Institute, Columbia University, New York, NY 10032, USA.

Table 1. Kinetic parameters and substrate preference for FHIT and PKCI (*7*). K_m, Michaelis constant; –, no product detected.

Protein	Substrate	K_m (μM)	k_{cat} (s^{-1})	k_{cat}/K_m (M^{-1} s^{-1})
FHIT	Ap_3A	65.0	2.3	3.5×10^4
FHIT	Ap_3A*	11.5	7.5	6.5×10^5
FHIT	Ap_3A†	65.0	0.038	5.8×10^2
FHIT	Ap_4A	31.3	0.10	3.2×10^3
FHIT	ATP	333	0.0025	7.5
FHIT	ADP	–		
PKCI	ADP	800	0.0068	8.5
PKCI	ATP	–		
PKCI	Ap_3A	–		

*With 1 mM $MgCl_2$. †With 1 mM EDTA.

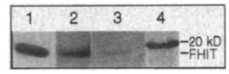

Fig. 1. Analysis of the covalent FHIT-nucleotide monophosphate intermediate by SDS-PAGE and autoradiography. Lane 1, cold unlabeled Coomassie blue–stained FHIT protein; lane 2, ^{32}P radiolabel coincident with the FHIT protein; lane 3, ^{3}H radiolabel coincident with the FHIT protein; lane 4, 10-kD ladder molecular weight markers. Details of the trapping reaction are summarized in the text (*10*).

modimers. The HIT protomer structure can be described as a general α + β type and further subclassed as an α + β meander fold (*2*, *3*). The HIT protomer contains a core of five antiparallel β strands and a central α helix. Two protomers are brought together in the homodimer through interactions between central helices and the joining of β strands into a 10-stranded antiparallel sheet. Histidine residues are prominent features in the two equivalent active sites of the HIT homodimer.

No enzymatic activity has been reported for PKCI or related subfamily members, although the rabbit PKCI HIT homolog has been shown to bind purine monophosphate nucleotides (*5*). However, FHIT and a related *Schizosaccharomyces pombe* HIT protein have been shown to cleave asymmetrically a broad range of dinucleotide polyphosphates in the presence of a divalent metal ion. These enzymes prefer an adenine base in the substrate with cleavage always resulting in the release of a monophosphate nucleotide (*6*). We now report that PKCI follows saturable kinetics in cleavage reactions with adenosine diphosphate (ADP) but not with Ap_3A or adenosine triphosphate (ATP), clearly showing a preference for an adenine base in the substrate (*7*). FHIT also cleaves ATP, Ap_3A, and Ap_4A with saturable kinetics, but not ADP (Table 1) (*8*). A metal binding site has not been identified in structures of either FHIT or PKCI (*2*, *3*, *5*), so we suspected that catalysis should occur in the absence of a divalent metal. Indeed, FHIT hydrolysis of Ap_3A proceeds, albeit at a slower rate, even in the presence of 1.0 mM EDTA (Table 1). If a divalent metal were required for hydrolysis, chelation would reduce the catalytic rate constant k_{cat} to an undetectable level, presumably zero. Nucleotide polyphosphates exist in the cell primarily as complexes with divalent cations. The metal ion effects observed here may result in part from the impact of divalent cations on nucleotide conformation.

Because a metal is not required and because of the conserved histidyl residues in the active site, we surmised that catalysis proceeds through a covalent nucleotidyl phosphohistidyl intermediate, as has been observed for many other enzymes (*9*). If this is true, a radiolabeled nucleotide [adenosine monophosphate (AMP)] should be found transiently and covalently attached to the protein. To confirm this hypothesis, we trapped a covalent FHIT-nucleotidyl phosphohistidyl intermediate in a hydrolase reaction using α-^{32}P– and 2,8-^{3}H–labeled ATP (*10*) (Fig. 1).

To elucidate the structural basis for HIT protein catalytic activity and to define characteristics of in vivo HIT ligands, we prepared a series of complexes representing key steps in the catalytic reaction. The PKCI and ADP catalytic cycle was characterized with the use of the nucleotide adenosine α/β-methylene diphosphate (AMP-CP) as an analog of the substrate complex. A transition-state analog was prepared by reacting the enzyme with adenosine and tungstate to produce the pentacovalent enzyme complex. Finally, the nucleotide product complex was produced by reacting the enzyme with AMP. Crystal structures of both FHIT and PKCI were determined for each of these complexes and were analyzed in comparison with the corresponding apo structures (*11*) (Table 2).

The apo unliganded structures (Figs. 2A and 3A) show FHIT His^{96} and PKCI His^{112} stabilized by a conserved structural motif. The carbonyl oxygen atom of FHIT His^{94} or PKCI His^{110} is hydrogen-bonded in a close interaction with the Nδ atom of FHIT His^{96} or PKCI His^{112}, suggesting the proper activation of these residues as nucleophiles for an in-line attack on the α phosphate group as it enters the binding pocket.

The substrate analog structures (Figs. 2B and 3B) of PKCI and FHIT in the presence of AMP-CP at 2.0 Å and 2.3 Å, respectively, show PKCI His^{112}, FHIT His^{96}, and ligand in an optimal orientation for attack at the α phosphate position. The distances to the phosphorus center from the Nε of PKCI His^{112} and from FHIT His^{96} are only 3.15 Å and 3.43 Å, respectively, whereas the distances to the proximal α phosphate oxygen atoms are nearly equal—an ideal situation for an in-line attack on the α phosphate group. The β phosphate group in the FHIT AMP-CP structure was disordered.

The transition-state analog structures (Figs. 2C and 3C) of PKCI and FHIT at 1.8 Å and 2.6 Å, respectively, show an adenosine base and tungstate ions bound in an orientation similar to that of the substrate analog. The transition-state analog structures are the

Table 2. Crystallographic data and refinement statistics (*11*).

	FHIT			PKCI		
	Apo	AMP-CP	Adenosine-tungstate	AMP	AMP-CP	Adenosine-tungstate
			Diffraction data			
d_{min}/λ (Å)	2.3/1.5418	2.3/1.0036	2.1/1.0740	1.4/1.5418	2.0/1.5418	1.8/1.5418
Unique reflections	16,062	17,347	17,675	36,893	26,213	43,312
Total reflections	100,846	71,374	167,167	158,000	194,693	318,416
Coverage (%)	94.6 (83.2)	95.7 (94.8)	79.6 (39.3)	84.5 (28.7)	71.5 (29.9)	84.3 (59.9)
R_{sym} (%)	7.6 (41.6)	3.3 (16.4)	6.4 (39.8)	6.2 (25.9)	5.6 (20.4)	8.5 (24.0)
			Refinement data			
Resolution	8 to 2.5 Å	8 to 2.3 Å	10 to 2.6 Å	8 to 1.5 Å	8 to 2.0 Å	10 to 1.8 Å
R/R_{free}	0.216/0.251	0.226/0.258	0.228/0.291	0.209/0.240	0.229/0.279	0.195/0.223
Number of reflections	12,031	16,087	10,338	32,145	24,149	40,772
Atoms (protein/water)	987/67	1028/48	1081/59	889/174	1775/122	1775/256

remarkable products of reacting the enzymes with adenosine and sodium tungstate, which resulted in the formation of three new covalent bonds: one between the Nε of PKCI His^{112} or FHIT His^{96} and the tungstate ion in the α phosphate position (bond length less than ~2.5 Å), one between the two tungstate ions, and one between the tungstate ion in the α phosphate position and the 5′-OH of the adenosine base. Two oxygen atoms are eliminated in the process. The tungstate ion in the α phosphate position is pentacovalent and has trigonal bipyramidal geometry (Fig. 4), thus mimicking the transition state for the α phosphate inversion during the first step of catalysis (*12*). As in the FHIT AMP-CP complex, the tungstate ion in the β phosphate position was disordered in the corresponding FHIT structure.

The product-bound structures (Figs. 2D and 3D) of PKCI and FHIT show characteristics of the final catalytic step. Although there are no gross differences in binding of the adenosine base among the three complexes of PKCI, there are differences in the binding of the α and β phosphate groups. In the 1.5 Å PKCI-AMP structure, the distance between Nε of His^{112} and the phosphorus atom in the α phosphate position is >3.5 Å. The orientation and binding of the oxygen atoms in the α phosphate position indicate interactions alternative to those observed in the previous two structures. Three structurally conserved water molecules (1W to 3W), located between the β strands behind the active-site histidines, are conserved in all FHIT and PKCI structures. An additional water within hydrogen-bonding distance to a phosphate oxygen, 4W, is found only in product (AMP) complexes of PKCI and FHIT.

This comprehensive structural and biochemical study has identified essential elements of the HIT protein catalytic cycle, leading us to propose a general mechanism for the

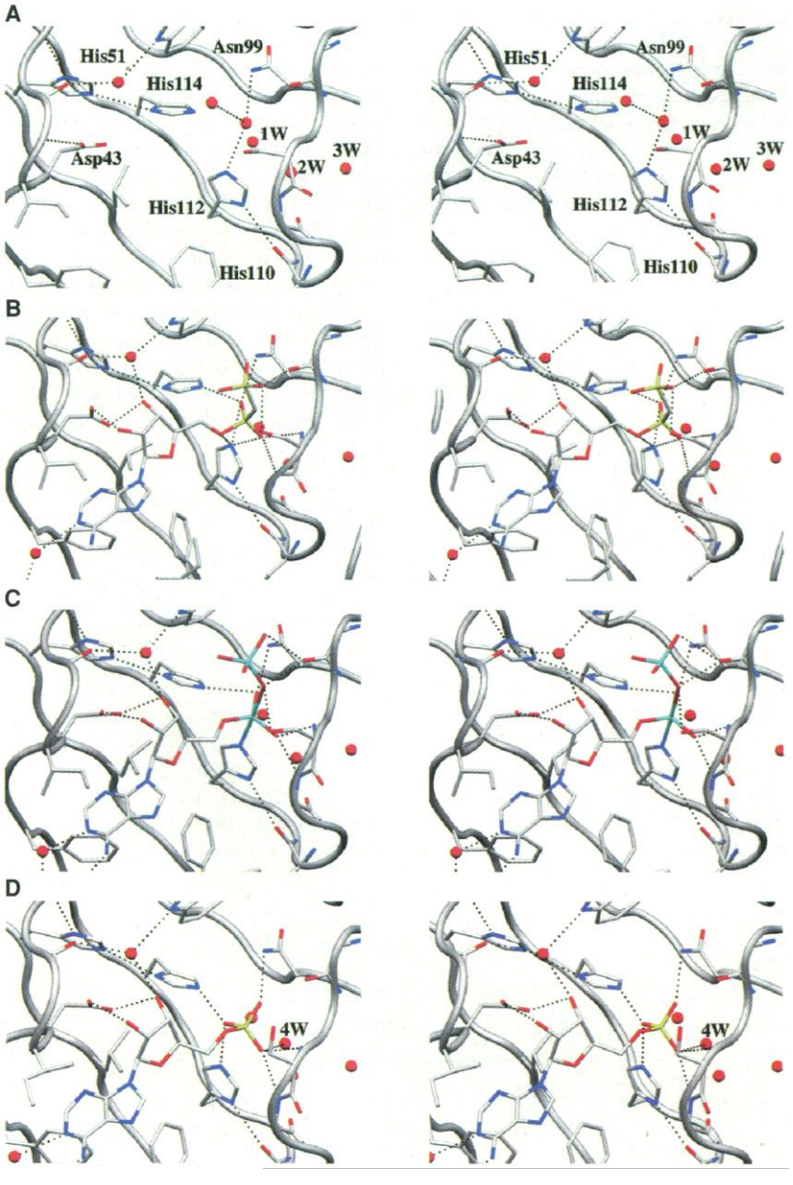

Fig. 2. Stereo views of PKCI in (**A**) apo, (**B**) AMP-CP substrate analog, (**C**) adenosine-tungstate transition-state analog, and (**D**) AMP product-bound forms. The region shown was selected to highlight interactions between the ligand and protein residues surrounding one of the two equivalent ligand-binding sites in the HIT homodimer. A subset of residues is shown superimposed on the Cα backbone cardinal spline of each respective structure. Hydrogen bonds are denoted by dotted lines. The tryptophan shown is in the COOH-terminal tail of the other protomer. Figure generated with Setor (*15*).

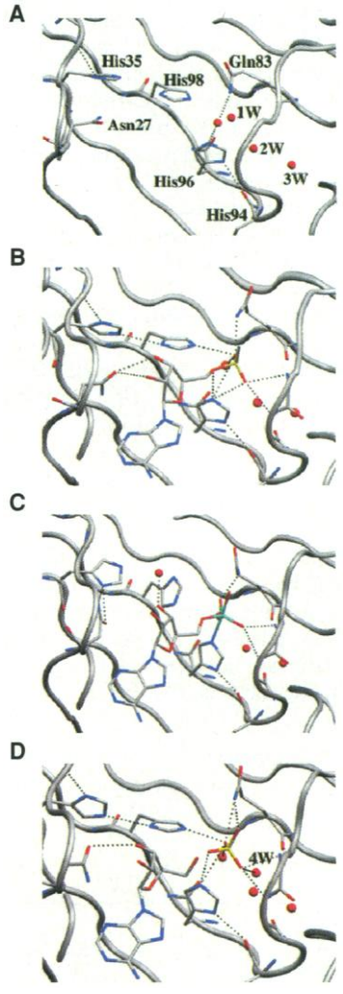

Fig. 3. Schematic diagram of FHIT in (**A**) apo, (**B**) AMP-CP substrate analog, (**C**) adenosine-tungstate transition-state analog, and (**D**) adenosine-sulfate product complexed forms. As in Fig. 2, hydrogen-bonding interactions are depicted by dotted lines. A subset of residues is shown superimposed on the Cα backbone cardinal spline of each respective structure.

HIT protein family (Fig. 5). One step of the catalytic cycle is missing from our structural study, that of the tetracovalent nucleotidyl intermediate (Fig. 5C). Thus, groups involved in activation of a second nucleophile for release of the product from the covalent histidyl complex are not readily apparent. However, the trapped covalent nucleotidyl phosphohistidyl intermediate (Fig. 1) serves as evidence of this catalytic step.

FHIT and PKCI bind ligand in a deep cleft in each protomer, the floor of which is formed from the five-stranded β sheet. Two structurally conserved loops located between the β strands of the floor are involved in direct contacts with the ligand. One loop is involved in side chain and backbone contacts with the phosphates of the ligand, and the other loop is involved in side chain contacts with the ribose and base of the ligand. The third side of the cleft is involved in contacts with the adenosine base and is formed by NH_2-terminal strands in the FHIT structure and by an NH_2-terminal helix in PKCI. The highly conserved COOH-terminal residues of PKCI mediate several PKCI-ligand interactions and form the fourth side of the cleft, a feature apparently absent in the FHIT structures. A loop between the last strand and helix of FHIT, although mostly disordered in the crystal structures, could be making PKCI-like contacts with the ligand during catalysis; such contacts are suggested by a comparison of the FHIT structures (*2*).

The highest degree of amino acid conservation between PKCI and FHIT is observed in the ligand-binding pocket and notably includes the conserved histidyl residues, two of which make direct contacts with the ligand α phosphate group. Although the nucleotide ribose and base occupy similar positions in PKCI and FHIT, few interactions observed in these complexes are mediated by conserved amino acid side chains. Analysis of the liganded states of these enzymes indicates that hydrogen-bonding distances between the protein and oxygen atoms in the α phosphate position are closer (by an average of ~0.3 Å, Luzzati coordinate error of 0.23) in the transition-state analog complexes (Figs. 2 and 3). The presumably stronger interactions could stabilize the inversion of the α phosphate when it passes through the pentacovalent transition state during catalysis.

FHIT histidyl residues, which face into a more open solvent-accessible cleft, are found to flip in response to the liganded state of the enzyme, possibly affecting the rate of hydrolysis and the determination of the unique substrate specificity for these two human HIT proteins. Despite this difference, catalysis at the α phosphate position appears to proceed in a similar manner in the two cases.

A recent analysis of the Protein Data Bank (PDB) (*13*) revealed that the PKCI dimer was structurally similar to a protomer of galactose-1-phosphate uridylyltransferase (*14*), also known as GalT. Subsequent reports also described features of this similarity (*2, 5*). The active site of GalT is also similar, but not identical, to that in HIT proteins. GalT catalyzes a phosphotransferase reaction, mediated through a covalent nucleotidyl phosphohistidyl intermediate, which involves the exchange of a uridine 5′-monophosphate moiety between the hexose-1-phosphates of glucose and galactose. This implies a functional as well as structural similarity to the HIT proteins.

Our results suggest that distant members within the HIT superfamily share a common catalytic mechanism; however, substrate specificity is likely dictated by the extent of divergence in the COOH-terminal residues, which vary greatly between HIT subfamilies. The catalytic activity observed in vitro is consistent with the ability of these enzymes to hydrolyze their substrates, whereas the covalent enzyme intermediates reported here suggest an alternative nucleotidyl phosphotransferase activity. Our studies support a mechanism by which the α phosphate of respective substrates undergoes an inversion through a trigonal bipyramidal pentacovalent transition state, thus resulting in a transient, covalently attached nucleotidyl protein intermediate before hydrolysis or transfer of the phosphoramidate bond. Although the in vivo substrates for both FHIT and PKCI remain undiscovered, the highly conserved and ubiquitous nature of the PKCI HIT subfamily throughout Archae, Prokaryae, and Eukaryae suggests a fundamental role for these closely related enzymes. The comparative structural biology approach undertaken here has identified an adenosine diphospho component of the ligand and identified differences between FHIT and PKCI that likely contribute to their unique activities. Similar structure-based approaches will become increasingly useful in the identification of protein function and mechanism as other protein families are revealed through the application of genomics.

Fig. 4. Stereo view of the 1.8 Å omit map (blue at 1.0σ) and Bijvöet difference map (red at 3.5σ) superimposed on the final PKCI substrate analog adenosine-tungstate structure. Note the trigonal bipyramidal geometry of the tungstate ion in the α phosphate position.

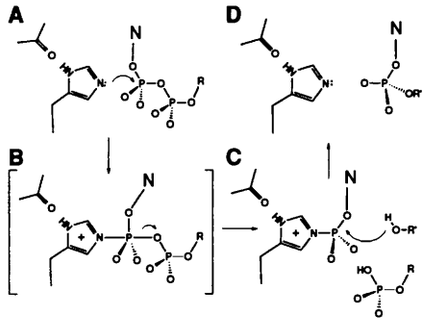

Fig. 5. Catalytic mechanism proposed for FHIT, PKCI, and (by analogy) all HIT family members. The α and β phosphate positions are depicted fully in the ligand. The positions of residues covalently attached to the phosphates are indicated by N, R, and R′, where N is the nucleoside, R is unknown for PKCI and known for several substrates for FHIT (Table 1), and R′ is a hydrogen in the hydrolysis reactions described for PKCI and FHIT (however, as observed for GalT, R′ may be another group in transferase reactions). (**A**) Substrate-bound form when the histidine acts as a nucleophile in an in-line attack on the α phosphate (AMP-CP structures). (**B**) Trigonal bipyramidal pentacovalent transition state of the inversion of the α phosphate position (adenosine-tungstate transition-state analog structures). (**C**) Covalently associated nucleotidyl phosphoprotein reaction intermediate (Fig. 1). (**D**) The product-bound form of the protein (AMP and adenosine-sulfate product-bound structures).

REFERENCES AND NOTES

1. B. Seraphin, *J. DNA Seq.* **3**, 177 (1992); K. Robinson and A. Aitken, *Biochem. J.* **304**, 662 (1994).
2. C. D. Lima *et al.*, *Structure* **5**, 763 (1997).
3. C. D. Lima, M. G. Klein, I. B. Weinstein, W. A. Hendrickson, *Proc. Natl. Acad. Sci. U.S.A.* **93**, 5355 (1996).
4. M. Ohta *et al.*, *Cell* **84**, 587 (1996). References to subsequent studies of the *FHIT* locus as related to human cancer can be found in (*2*).
5. C. Brenner *et al.*, *Nature Struct. Biol.* **4**, 231 (1997).
6. A. K. Robinson, C. E. Pena, L. D. Barnes, *Biochim. Biophys. Acta* **1161**, 139 (1993); L. D. Barnes *et al.*, *Biochemistry* **36**, 11529 (1996).
7. A systematic approach was used to identify adenosine as the nucleoside with highest affinity for the binding site by soaking pairs of various nucleoside molecules into the crystal in equal concentrations (~0.1 to 1.0 mM), collecting data, and observing density in the binding site. Adenosine nucleosides were always found to bind to PKCI with higher affinity than any other nucleoside.
8. Nanomolar concentrations of FHIT were incubated with 5 to 160 × 10^{-6} M Ap_4A and Ap_3A for 30 min. Submicromolor concentrations of FHIT were incubated with 50 to 1600 × 10^{-6} M ADP and ATP for

180 min. All reactions were conducted in 100 μl of 10 mM Hepes (pH 7.5) at 37°C. Cleavage products were analyzed with a Waters high-performance liquid chromatograph and DEAE column using a gradient elution of 50 mM ammonium phosphate (pH 5.2) to 450 mM ammonium phosphate (pH 5.7) (*6*). PKCI hydrolysis reactions were conducted as above with ADP, AppA, and ATP as substrates. AppA hydrolysis was qualitatively observed for PKCI, as was 7-methyguanosine 5′-triphospho-5′-adenosine and Ap_5A hydrolysis for FHIT.

9. Y. F. Wei and H. R. Matthews, *Methods Enzymol.* **200**, 388 (1991); S. J. Pilkis *et al.*, *J. Biol. Chem.* **258**, 6135 (1983); C. A. Hasemann, E. S. Istvan, K. Uyeda, J. Deisenhofer, *Structure* **4**, 1017 (1996); Z. B. Rose, *Methods Enzymol.* **87**, 42 (1982); S. H. Thrall, A. F. Mehl, L. J. Carroll, D. Dunaway-Marino, *Biochemistry* **32**, 1803 (1983); S. Morera, M. Chiadmi, G. LeBras, I. Lascu, J. Janin, *ibid.* **34**, 11062 (1995); J. E. Wedekind, P. A. Frey, I. Rayment, *ibid.* **35**, 11560 (1996).
10. FHIT protein (5 μg) was incubated in 100-μl reactions with 50 μM unlabeled ATP spiked with 0.033 μM [α-^{32}P]ATP (~3000 Ci/mmol) or with 0.033 μM [2,8-^{3}H]ATP (25 to 40 Ci/mmol). The reaction was stopped after 60 min by precipitation and denaturation by addition of 10% trichloroacetic acid (TCA) [bovine serum albumin (0.5 μg/μl) as carrier]. The pellet was resuspended in 0.1 N NaOH, reprecipitated with 10% TCA, and finally resuspended in 100 mM ammonium bicarbonate, pH 9 (*9*). The reaction was boiled in SDS sample buffer and loaded onto a 17.5% SDS–polyacrylamide gel electrophoresis (PAGE) gel for analysis. The radioactive bands in Fig. 4 were detected by film autoradiography over 6 hours (α-^{32}P) and 12 weeks (2,8-^{3}H). A similar approach was used to trap covalent phosphotyrosine intermediates in topoisomerase reactions [Y.-C. Tse-Dinh, K. Kirkegaard, J. Wang, *J. Biol. Chem.* **255**, 5560 (1980)]. Radioactive labeling was coincident with the position of FHIT in SDS-PAGE.
11. $R_{sym} = \Sigma|I - \langle I\rangle|/\Sigma I$, where I = observed intensity and $\langle I\rangle$ = average intensity; the crystallographic R factor is based on 95% of the data used in refinement and R_{free} is based on 5% of the data withheld for the cross-validation test. Unique reflections distinguish Bijvoet mates. All other statistics on refinement and diffraction data can be found in the respective PDB entries (codes: 4FIT, 5FIT, 6FIT, 1KPE, 1KPF, and 1AV5). FHIT and PKCI protein expression and purification were as described (*2*, *3*). Crystallization of the various complexes is described in the PDB entries. The FHIT–AMP-CP complex was collected and processed at the Advanced Photon Source (APS) Structural Biology Center (SBC) undulator beamline 19-ID on the charge-coupled device detector [E. M. Westbrook and I. Naday, *Methods Enzymol.* **276**, 244 (1997); M. L. Westbrook, T. A. Coleman, R. T. Daley, J. W. Pflugrath, in *Proceedings of IUCr Computing School*, P. E. Bourne and K. Watenpaugh, Eds. (SDSC Inc., San Diego, CA, 1996)]. The FHIT adenosine-tungstate data were collected at the NSLS beamline X4A at the peak of the LII edge of tungsten in order to optimize the anomalous signal from the bound tungstate. All other data were collected on a RAXISII and processed with the programs DENZO and SCALEPACK [Z. Otwinowski and W. Minor, *Methods Enzymol.* **276**, 307 (1997)]. Subsequent data reduction was done with the CCP4 suite of programs [SERC (UK) Collaborative Computing Project 4 (Daresbury Laboratory, Warrington, UK, 1979)]. Although five of the reported structures all crystallized in previously reported space groups (*2*, *3*), the PKCI-AMP complex crystallized in an alternative space group ($P4_32_12$) and was solved using a partial model (*3*) in molecular replacement with AMORE [J. Navaza, *Acta Crystallogr.* **A50**, 157 (1994)] and modeled with the program O [T. A. Jones, J. Y. Zou, S. W. Cowan, M. Kjeldgaard, *ibid.* **A47**, 110 (1991)]. Isomorphous, related space groups were solved by a similar approach in AMORE. All models were refined with X-Plor using the cross-validation test [A. T. Brünger, J. Kuriyan, M. Karplus, *Science* **235**, 458 (1987); A. T. Brünger, *Nature* **355**, 472 (1992)]. Each FHIT model roughly includes residues 2 to 108 and 125 to 147. Each PKCI model roughly includes residues 14 to 126. Occupancies for the α and β tungstate molecules refined to 0.50 and 0.54, respectively, for PKCI and to 0.47 for FHIT.
12. Vanadate and molybdate pentacovalent metal sites were identified in structures of chloroperoxidase, rat acid phosphatase, bovine low-molecular weight phosphotyrosyl phosphatase, ribonuclease A, and a vanadate-ADP transition-state complex of S1 myosin [B. Borah *et al.*, *Biochemistry* **24**, 2058 (1985); Y. Lindqvist, G. Schneider, P. Vihko, *Eur. J. Biochem.* **221**, 139 (1994); A. Messerschmidt and R. Wever, *Proc. Natl. Acad. Sci. U.S.A.* **93**, 392 (1996); C. A. Smith and I. Rayment, *Biochemistry* **35**, 5404 (1996); A. Wlodawer, M. Miller, L. Sjolin, *Proc. Natl. Acad. Sci. U.S.A.* **80**, 3628 (1983); M. Zhang, M. Zhou, R. L. Van Etten, C. V. Stauffacher, *Biochemistry* **36**, 15 (1997)]. The active sites of PKCI and FHIT share several structural similarities and characteristics with protein phosphatases, particularly rat acid phosphatase. A search of the small-molecule database revealed a pentacovalent tungstate structure with similar characteristics to those observed in our enzyme complex [I. Feinstein-Jaffe, J. C. Dewan, R. R. Schrock, *Organometallics* **4**, 1189 (1985)]. The bond lengths and angles observed in our crystal structures are in agreement with those observed in several other tungsten-containing molecules found in the database. We know of no reported protein structure that describes a similar pentacovalent tungstate complex.
13. L. Holm and C. Sander, *Structure* **15**, 165 (1997); *Trends Biochem. Sci.* **22**, 116 (1997).
14. J. E. Wedekind, P. A. Frey, I. Rayment, *Biochemistry* **34**, 11049 (1995).
15. S. V. Evans, *J. Mol. Graphics* **11**, 134 (1993).
16. We thank the staffs of beamline X4A at the National Synchrotron Light Source (NSLS) and beamline 19-ID at the APS. We particularly thank members of the Hendrickson lab for helpful discussion, and especially C. Bingman for discussions about catalysis. We also thank the Pyle, McDermott, and Parkin labs for helpful discussions and for use of resources during the analysis of the catalytic intermediate. Beamline X4A at the NSLS, a U.S. Department of Energy facility, is supported by the Howard Hughes Medical Institute. Use of the APS was supported by the U.S. Department of Energy, Basic Energy Sciences, Office of Energy Research. The SBC is supported by the U.S. Department of Energy, Office of Health and Environmental Research, Office of Energy Research. Both the SBC and APS are supported under contract W-31-109-ENG-38. This work was supported in part by National Cancer Institute training grant T32CA09503 (M.G.K.) and by a Helen Hay Whitney Foundation Fellowship to C.D.L.

3 April 1997; accepted 4 September 1997

Angiogenic and HIV-Inhibitory Functions of KSHV-Encoded Chemokines

Chris Boshoff,* Yoshio Endo, Paul D. Collins, Yasuhiro Takeuchi, Jacqueline D. Reeves, Vicki L. Schweickart, Michael A. Siani, Takuma Sasaki, Timothy J. Williams, Patrick W. Gray, Patrick S. Moore, Yuan Chang, Robin A. Weiss

Unique among known human herpesviruses, Kaposi's sarcoma–associated herpesvirus (KSHV or HHV-8) encodes chemokine-like proteins (vMIP-I and vMIP-II). vMIP-II was shown to block infection of human immunodeficiency virus–type 1 (HIV-1) on a CD4-positive cell line expressing CCR3 and to a lesser extent on one expressing CCR5, whereas both vMIP-I and vMIP-II partially inhibited HIV infection of peripheral blood mononuclear cells. Like eotaxin, vMIP-II activated and chemoattracted human eosinophils by way of CCR3. vMIP-I and vMIP-II, but not cellular MIP-1α or RANTES, were highly angiogenic in the chorioallantoic assay, suggesting a possible pathogenic role in Kaposi's sarcoma.

Kaposi's sarcoma (KS) is a highly angiogenic multicentric tumor most commonly seen in immunodeficient individuals. Since the acquired immunodeficiency syndrome (AIDS) epidemic, KS has become one of the most common tumors in parts of Africa and is the most common tumor found in HIV-infected individuals (*1*). Compared to classic KS found in patients from Mediterranean or East European descent, KS in AIDS patients is a more fulminant disease: The angiogenic properties of the HIV-1 Tat protein have been proposed to enhance KS tumor formation (*2*).

KSHV DNA is present in all KS biopsies, and antibodies to this virus are detectable mainly in those with KS or at risk of developing KS (*3*). These data, and previous epidemiological data indicating that an infectious agent is involved in KS pathogenesis (*4*), suggest that KSHV is likely to

C. Boshoff, Y. Takeuchi, J. D. Reeves, R. A. Weiss, Institute of Cancer Research, Chester Beatty Laboratories, London SW3 6JB, UK.
Y. Endo and T. Sasaki, Department of Experimental Therapeutics and Development Center for Molecular Target Drugs, Cancer Research Institute, Kanazawa University, Japan.
P. D. Collins and T. J. Williams, Department of Applied Pharmacology, Imperial College School of Medicine at National Heart and Lung Institute, London SW3 6LY, UK.
V. L. Schweickart and P. W. Gray, ICOS, 22021 20th Avenue Southeast, Bothell, WA 98021, USA.
M. A. Siani, Gryphon Sciences, San Francisco, CA 94080, USA.
P. S Moore and Y. Chang, Department of Pathology and Epidemiology, College of Physicians and Surgeons of Columbia University, New York, NY 10032, USA.

*To whom correspondence should be addressed.